

Some tests of an approximate density functional for the ground-state kinetic energy of a fermion system

Conyers Herring and Manoj Chopra

Department of Applied Physics, Stanford University, Stanford, California 94305

(Received 17 August 1987)

Any proposed approximation to the ground-state kinetic energy of a system of noninteracting fermions in terms of the particle density $\rho(\mathbf{r})$ can be used to estimate the potential field $v(\mathbf{r})$ that will give rise to a given $\rho(\mathbf{r})$, or the $\rho(\mathbf{r})$ that will result from placing a given number of particles in a given $v(\mathbf{r})$. Comparison with exact quantum-mechanical calculations thus gives two possible types of tests for any proposed kinetic-energy functional. This paper reports such tests for a recently proposed nonlocal functional applicable to one-dimensional systems, comparing its predictions for several simple problems not only with the correct answers but also with the predictions of Thomas-Fermi and Thomas-Fermi-Weizsäcker functionals, to which the new functional proves considerably superior. The comparisons yield useful insights on the virtues and defects of the new functional, and on the directions in which improvements should be sought. Particular attention is devoted to Friedel oscillations and shell structure. It is shown that functionals of the Thomas-Fermi-Weizsäcker type can never predict multiple maxima in ρ if v has only a single minimum and no maxima; the new functional does not have this defect, though it yields density oscillations rather weaker than the exact quantum-mechanical calculations. A natural general inference from the present tests is that any satisfactory kinetic-energy functional must (as ours does) replace the entire Thomas-Fermi term by a nonlocal expression.

I. INTRODUCTION

A previous paper¹ has discussed the problem of expressing the ground-state kinetic energy of a many-fermion system as a functional of the single-particle density distribution and has argued that for an approximation to such a functional to be sufficiently accurate to be useful in typical practical problems, it must be fully nonlocal. Some general desiderata for such a kinetic-energy functional were developed, and for the special case of one-dimensional problems a particular functional with promising characteristics was chosen for evaluation on a number of examples. This functional approximates the minimum total kinetic energy T consistent with a given density distribution $\rho(x,s)$ for particles of each spin s , by the quantity \tilde{T} , defined as

$$\tilde{T} = \sum_s \left[T_w \{ \rho(x,s) \} + \frac{\pi^2}{6} \int_{\bar{x}_{\min}(s)}^{\bar{x}_{\max}(s)} \frac{d\bar{x}}{[\xi_1(\bar{x},s)]^2 \Delta x(\bar{x},s)} \right], \tag{1}$$

where T_w is the Weizsäcker energy defined as

$$T_w = \frac{1}{8} \int_{-\infty}^{\infty} \frac{|d\rho(x,s)/dx|^2 dx}{\rho(x,s)} \tag{2}$$

for spin s , and where for each s the integral is over the set of all one-particle intervals x' to $x'+\Delta x = x''$, each labeled by its midpoint

$$(x' + x'')/2 = \bar{x}, \tag{3}$$

and with

$$\int_{x'}^{x''} \rho(x,s) dx = 1, \tag{4}$$

$$\int_{x'}^{x''} \frac{dx}{\rho(x,s)} = \xi_1^2. \tag{5}$$

In Ref. 1 the quantity ξ_1 was called the “remoteness” of x'' from x' , since it becomes large when there is a high potential barrier between them. The upper and lower limits of \bar{x} , \bar{x}_{\max} , and \bar{x}_{\min} , respectively, are normally $\pm\infty$, but may be finite if there are impenetrable constraining walls. Atomic units ($\hbar = m = 1$) are used for brevity. In the earlier paper (Ref. 1, Table I) this functional was shown to give kinetic energies for a wide variety of problems within a few percent of the correct ones. The object of the present paper is to explore the accuracy with which one can infer from the approximation (1) either the single-particle potential $v(x)$ from which a given density distribution was derived, or the density that arises from placing a given number of particles in a given potential. Since for each problem this is a comparison of the entire course of a calculated function with the correct function, it is a much more informative test than the calculation of the total energy, which is a single number for each problem. It will thus reveal shortcomings of the present approximation and call attention to ways in which it needs improvement.

As was noted in Secs. IB and IC of Ref. 1, practical problems are usually solved by a self-consistent-field procedure in which one computes a series of successive approximations to the particle density and to the effective single-particle potential. The quantum-mechanical aspects of an approximation procedure can be introduced either in the determination of the density going with a

given potential, or in the determination of the potential needed to produce a given density. Since our approximation (1) is formulated in terms of a given input density $\rho(x,s)$, the second, or " $\rho \rightarrow v$ " procedure is the one that is more easily implemented. We shall devote Sec. II to the derivation of an explicit expression for the variational derivative of the kinetic-energy expression (1) with respect to the density, which, as discussed in Sec. I B of Ref. 1 is, to within an arbitrary additive constant, the negative of the single-particle potential which would yield the given density. In Sec. III we shall present explicit evaluations of this expression for the particle densities of a number of problems whose exact wave-mechanical solutions are known—specifically, some of the ones described in connection with Table I and Fig. 4 of Ref. 1. These will be compared not only with the correct potentials, i.e., those used for the wave-mechanical solutions, but also with the potentials that would be inferred from the Thomas-Fermi approximation, with or without gradient corrections. Section IV will take up the more difficult but perhaps more interesting problem of determining the density corresponding to a given single-particle potential. To compute this using the scheme of Eq. (1), it will be necessary to proceed by successive approximations, a rather laborious procedure, though no more laborious than what always has to be done for real-world problems where the effective single-particle potential is not known at the outset. Section V will summarize some of the lessons to be learned from these comparisons.

II. THE POTENTIAL AS A VARIATIONAL DERIVATIVE

A. Potential resulting from the approximation (1)

Let us consider the first-order variation of the two terms of (1) when a small variation $\delta\rho(x,s)$ is made in the density. If the variation is reduced to the form

$$\delta\bar{T} = - \sum_s \int_{-\infty}^{\infty} \bar{v}(x,s) \delta\rho(x,s) dx, \quad (6)$$

then $\bar{v}(x,s)$ can be interpreted as the effective single-particle potential for particles of spin s as given by the starting approximation (1), since if the approximations were indeed exact, \bar{v} would be the true single-particle po-

tential. Since we shall be considering only problems in which the potential is the same for both spins, we shall henceforth consider only particles of a single spin and for brevity shall drop the spin index s .

The two terms in (1) give separate contributions v_w and \bar{v}_θ to \bar{v} . The former, or Weizsäcker, contribution can be written down at once: It is [cf. Eq. (11) of Ref. 1]

$$v_w = \frac{1}{4\rho} \frac{d^2\rho}{dx^2} - \frac{1}{8\rho^2} \left[\frac{d\rho}{dx} \right]^2. \quad (7)$$

To evaluate the contribution \bar{v}_θ , we first need the variations of Δx and ξ_1^2 . These involve $\delta\rho$ not only directly but also through its effect on x' and x'' . For fixed \bar{x} , we have from (3)

$$\delta x' + \delta x'' = 0 \quad (8)$$

and from (4),

$$\rho(x'')\delta x'' - \rho(x')\delta x' + \int_{x'}^{x''} \delta\rho(x) dx = 0. \quad (9)$$

From these and (5) we obtain

$$\begin{aligned} \delta(\Delta x) &= \delta x'' - \delta x' \\ &= 2\delta x'' = -2[\rho(x'') + \rho(x')]^{-1} \int_{x'}^{x''} \delta\rho dx, \end{aligned} \quad (10)$$

$$\begin{aligned} \delta(\xi_1^2) &= \frac{\delta x''}{\rho(x'')} - \frac{\delta x'}{\rho(x')} - \int_{x'}^{x''} \frac{\delta\rho dx}{\rho^2} \\ &= -\frac{1}{\rho(x')\rho(x'')} \int_{x'}^{x''} \delta\rho dx - \int_{x'}^{x''} \frac{\delta\rho dx}{\rho^2}. \end{aligned} \quad (11)$$

Inserting these in the variation of the second term of (1) gives a double integral on x and \bar{x} in which $\delta\rho$ occurs only as $\delta\rho(x)$.

To extract $\bar{v}_\theta(x)$ as the coefficient of $\delta\rho(x)$ in this last expression, we must interchange the order of integration on x and \bar{x} . Since for each \bar{x} , x runs from $x'(\bar{x})$ to $x''(\bar{x})$, the region of integration in the $x\bar{x}$ plane is the hatched area of Fig. 1. When the order of integration is interchanged, the range of \bar{x} for a given x is from a lower limit $x_a(x)$ to an upper limit $x_b(x)$ as shown. The coefficient of $\delta\rho(x)$ in the subsequent integration on x gives, on insertion of the factor $-\pi^2/6$, the desired quantity $\bar{v}_\theta(x)$:

$$\begin{aligned} \bar{v}_\theta(x) &= -\frac{\pi^2}{6} \left\{ \int_{x_a(x)}^{x_b(x)} \frac{d\bar{x}}{[\xi_1(\bar{x})]^2 \Delta x(\bar{x})} \left[\frac{2}{\Delta x(\bar{x})[\rho(x') + \rho(x'')] } + \frac{1}{[\xi_1(\bar{x})]^2 \rho(x')\rho(x'')} \right] \right. \\ &\quad \left. + \frac{1}{[\rho(x)]^2} \int_{x_a(x)}^{x_b(x)} \frac{d\bar{x}}{[\xi_1(\bar{x})]^4 \Delta x(\bar{x})} \right\}. \end{aligned} \quad (12)$$

The expression (12) is easily evaluated numerically for any given function $\rho(x)$ using the definitions (3), (4), and (5). Note that since the integrands in (12) do not depend on x , the values of the integrals for any x can be derived from those for a neighboring x by addition of the increments due to changes of the limits.

Note that the approximation (12) reproduces an important property known to be possessed by the true $v_\theta(x)$, that it is everywhere less than or equal to its value at infinity.²

Since one of the conditions imposed in obtaining the approximate functional (1) was that it should give the

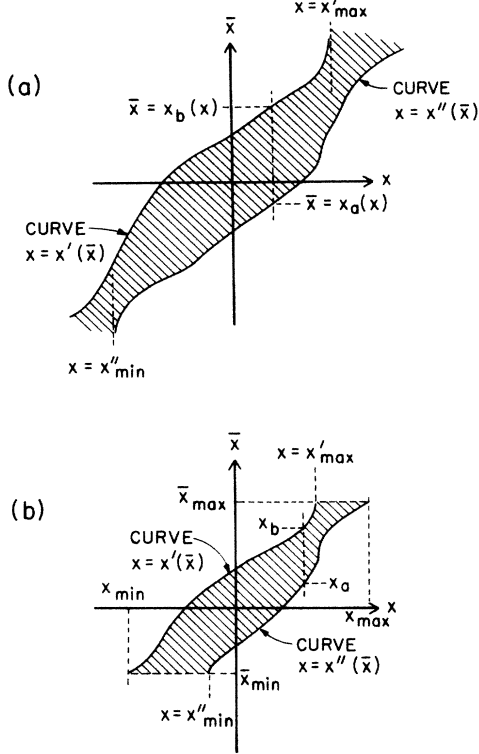


FIG. 1. Region of integration (hatched) for the double integral on x and \bar{x} that results when (11) is inserted into the second term of (1): (a) for a density $\rho(x)$ that decays gradually to zero as $x \rightarrow \pm\infty$, (b) for a density confined between impenetrable barriers at $x = x_{\min}$ and $x = x_{\max}$.

correct kinetic energy when the density is uniform or departs from uniformity only slightly in a Fermi wavelength, we would expect expression (12) to be exactly correct in the limit of uniform ρ . Indeed one finds that if $\rho = \rho_0$, $\Delta x = 1/\rho_0$, $\xi_1^2 = 1/\rho_0^2$, and

$$\bar{v}_\theta = -\pi^2 \rho_0^2 / 2, \quad (13)$$

which is the correct value.

B. Approximate linear response in position space

In the search for satisfactory approximations \tilde{T}_θ to the non-Weizsäcker part T_θ of the kinetic energy, a

$$\begin{aligned} \text{Curly bracket} = & 3\rho_0^2 - 2\rho_0\rho_1(x) - \frac{3}{2}\rho_0^2 \int_{x-1/\rho_0}^{x+1/\rho_0} \rho_1(x_1) dx_1 \\ & - \frac{3}{2}\rho_0^2 \int_{x-1/2\rho_0}^{x+1/2\rho_0} d\bar{x} [\rho_1(\bar{x} - 1/2\rho_0) + \rho_1(\bar{x} + 1/2\rho_0)] + 14\rho_0^3 \int_{x-1/2\rho_0}^{x+1/2\rho_0} d\bar{x} \int_{\bar{x}-1/2\rho_0}^{\bar{x}+1/2\rho_0} \rho_1(x_1) dx_1. \end{aligned} \quad (20)$$

The last double integral can be converted to a single integral by interchanging the order of integration, so that all terms of (20) beyond the first two take the form of integrals on x_1 of $\rho_1(x_1)$ times simple functions of $(x - x_1)$. After final collection of terms, the \bar{v}_θ of (12) reduces in first order to an expression of the form (15), with

search which led to the second term of (1) as a plausible candidate, one of the criteria used was that the approximate \bar{v}_θ should agree as closely as possible with the true v_θ for the case of an almost constant particle density whose nonuniformities are treated to first order.²⁶ A comparison of the Fourier coefficients of v_θ and the present \bar{v}_θ was given in Fig. 3 of Ref. 1. Possession of the explicit expression (12) now enables us to make the corresponding comparison in coordinate space. Thus, if, for a single spin,

$$\rho(x) = \rho_0 + \rho_1(x), \quad (14)$$

with ρ_0 constant and ρ_1 small, we can write to first order

$$\begin{aligned} \bar{v}_\theta(x) = & v_0 \left[1 + \bar{A} \rho_1(x) / \rho_0 \right. \\ & \left. + \int \bar{Q}(2k_F |x - x'|) \rho_1(x') dx' \right] \end{aligned} \quad (15)$$

and a corresponding equation for $v_\theta(x)$ obtained by omitting the tildes in (15); here v_0 is the Thomas-Fermi potential $-\pi^2 \rho_0^2 / 2$ for density ρ_0 , measured relative to a zero at the Fermi energy. To evaluate the constant \bar{A} and the \bar{Q} from (12), we must use the first-order expressions for $\Delta x(\bar{x})$ and $\xi_1^2(\bar{x})$. These are easily found to be

$$\Delta x = \frac{1}{\rho_0} - \frac{1}{\rho_0} \int_{\bar{x}-1/2\rho_0}^{\bar{x}+1/2\rho_0} \rho_1(x_1) dx_1, \quad (16)$$

$$\xi_1^2 = \frac{1}{\rho_0^2} - \frac{2}{\rho_0^2} \int_{\bar{x}-1/2\rho_0}^{\bar{x}+1/2\rho_0} \rho_1(x_1) dx_1. \quad (17)$$

The first-order expressions for the limits of integration are

$$x_a = x - \frac{1}{2\rho_0} + \frac{1}{2\rho_0} \int_{x-1/\rho_0}^x \rho_1(x_1) dx_1 \quad (18)$$

and

$$x_b = x + \frac{1}{2\rho_0} - \frac{1}{2\rho_0} \int_x^{x+1/\rho_0} \rho_1(x_1) dx_1. \quad (19)$$

With use of (16)–(19) the first-order expression for the curly-bracket expression in (12) becomes, after partial collection of terms,

$$\bar{A} = -\frac{2}{3}, \quad (21)$$

$$\bar{Q}(2k_F |x - x'|) \equiv \bar{Q}(u) = \begin{cases} \frac{11}{3} - \frac{7|u|}{3\pi} & (|u| \leq 2\pi) \\ 0 & (|u| > 2\pi). \end{cases} \quad (22)$$

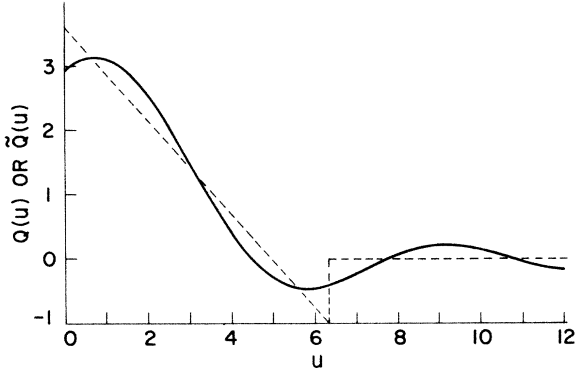


FIG. 2. Exact and approximate forms for the position-space linear-response kernel in one dimension, defined by (15). Full curve, correct kernel $Q(u)$ [Ref. 1, Fig. 2(a) and Appendix A]; dashed curve, kernel $\tilde{Q}(u)$ given by (22), corresponding to the approximate \tilde{T} of (1).

These may be compared with the corresponding quantities for the linear-response behavior of the exact v_θ , namely,⁴ $A = -\frac{2}{3}$ and the function $Q(u)$ plotted as the smooth curve in Fig. 2. It will be seen that \tilde{Q} gives about as good a representation of Q as one could get with a function of finite range and simple triangular shape, but lacks certain fine features, especially the grad-

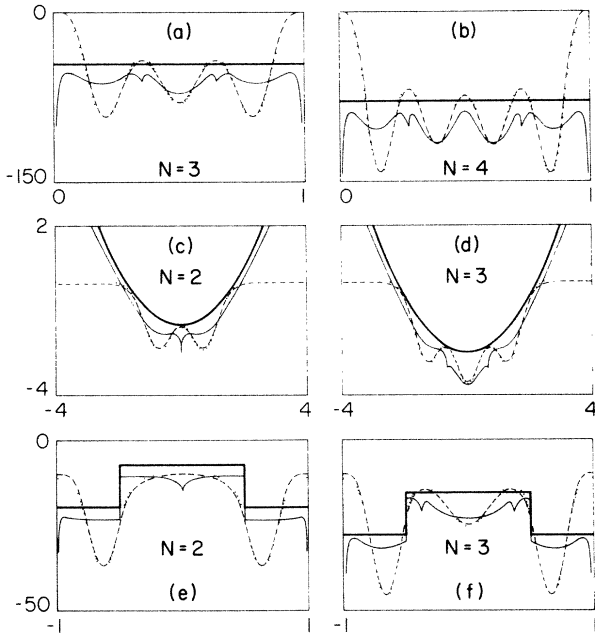


FIG. 3. Sample comparisons of the “true” potentials $v(x)$ from which each of a number of densities $\rho(x)$ were generated for N noninteracting particles by wave mechanics (dark curves), the corresponding approximate potentials $\bar{v}(x)$ generated from the same $\rho(x)$ by evaluation of (12) and (7) (light solid curves), and the more familiar approximations $v_{TF}(x)$ [Eq. (23), dashed curves] and $v_{TF}(x) + v_w(x)/9$ (dotted curves). Plots (a) and (b), box with impenetrable walls. Plots (c) and (d), harmonic oscillator. Plots (e) and (f), box with impenetrable walls at $x = \pm 1$ and a square barrier of finite height from $x = -\frac{1}{2}$ to $\frac{1}{2}$.

ually decaying long-range oscillations. The latter defect is related to the failure of the corresponding approximate response function in Fourier space³ to reproduce the sharp singularity of the correct response function at wave vector $2k_F$. Correction of this defect would require use of a functional involving density correlations of longer range than a one-particle interval, e.g., two-, three-, etc. particle intervals.

III. POTENTIAL FOR SOME GIVEN DENSITIES

A. General course of $\bar{v}_\theta(x)$

The integral (12) for the function $\bar{v}_\theta(x)$ was evaluated numerically for a number of different densities $\rho(x)$ corresponding to the exact quantum-mechanical ground states of two, three, or four parallel-spin noninteracting particles in various simple potentials $v(x)$. Each such $\bar{v}_\theta(x)$ was then added to the $v_w(x)$ given by (7) to yield $\bar{v}(x)$, our suggested approximation to the true potential $v(x)$ associated with the given density distribution. Figure 3 shows, for six sample densities (graphs of these densities are given in Fig. 4 of Ref. 1), the comparisons of $\bar{v}(x)$ (light solid curves) with $v(x)$ (dark solid curves). Also shown are plots of the potential $v_{TF}(x)$ given by Thomas-Fermi theory, namely,

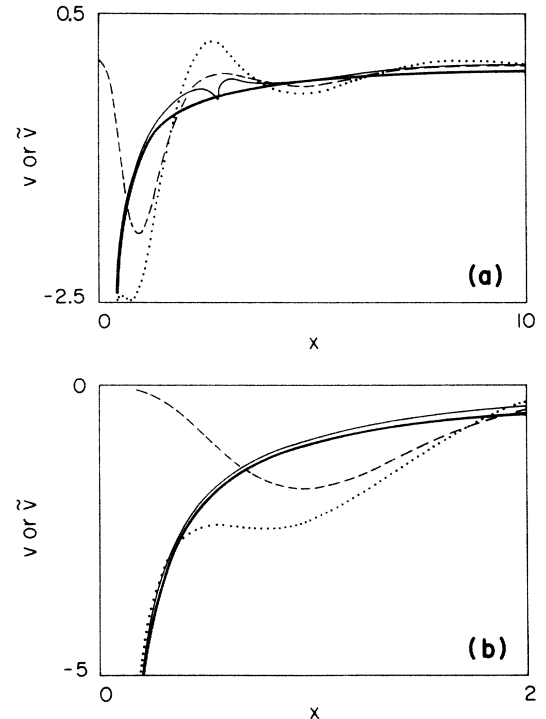


FIG. 4. Comparisons, as in Fig. 3, of different potentials associated with the radial density $\rho(x)$ of three noninteracting particles in the 1s, 2s, and 3s states of an attractive Coulomb potential. Shown are the “true potential” $v = -1/x$ used to generate $\rho(x)$ (dark curve), the approximate potential \bar{v} of (12) plus (7) (light solid curve), the v_{TF} of (23) (dashed curve), and v_{TF} plus the full v_w of (7) (dotted curve). Plots (a) and (b) show the range of large and small x , respectively.

$$v_{TF}(x) = -\pi^2[\rho(x)]^2/2 \quad (23)$$

(dashed curves), and plots of the sum $v_{TF}(x) + v_w(x)/9$ (dotted curves). Figure 4 shows a similar comparison for potentials derived from the radial density of three parallel-spin particles occupying the 1s, 2s, and 3s states of a Coulomb potential. (This problem, incidentally, can be related to that of a highly ionized atom with occupied s, p, and d shells, thanks to a theorem due to March.⁵)

A word of explanation is in order regarding the vertical positioning of the curves. If one merely requires of $v(x)$ that it give rise to the given $\rho(x)$, then $v(x)$ and $v(x)$ plus any arbitrary constant are equally acceptable. However, we may remove this arbitrariness by defining, for the exact kinetic-energy function $T\{\rho\}$ or for any approximation $\tilde{T}\{\rho\}$ to it,

$$v(x) = -[\delta T/\delta\rho(x)]_-, \quad \bar{v}(x) = -[\delta\tilde{T}/\delta\rho(x)]_-, \quad (24)$$

where the subscript minus sign means that the variational derivative, which for the exact case is discontinuous across any surface in density-parameter space corresponding to an integral total number of particles,⁶ is to be evaluated on the low-number side of such a surface. With this definition $v(x)$ is referred to a zero at the level of the energy of the highest occupied single-particle state. This convention has been used for the $v(x)$ curves in Fig. 3, but not in Fig. 4, where its use would shift the $v(x)$ curve upward by $\frac{1}{18}$ hartree and make it almost hide some of the other curves at large x .

Let us consider for the present just the shapes of the curves in Figs. 3 and 4, without regard to their absolute vertical positions. Several aspects of these shapes are worth noting.

(i) The Thomas-Fermi potential v_{TF} has two major defects: It oscillates rather wildly because of the oscillation in ρ , even when the true $v(x)$ is fairly smooth, and it becomes flat at the value zero (i.e., the Fermi energy) in the tails where ρ is small if v is going to infinity.

(ii) Adding a fraction of the Weizsäcker potential v_w to v_{TF} improves the behavior in the tails, but at the cost of worsening the oscillatory behavior. Since v_w is known to approach the correct v in the tails,⁷ addition of the full v_w would give an excellent approximation here, but usually horrible oscillations elsewhere.

(iii) The \bar{v} obtained from (12) and v_w represents the true v very well in two types of regions: In the tail regions, where v exceeds the energy of the highest occupied single-particle state and where the necessity for quantum-mechanical tunneling has reduced the density to a low value, and in Fig. 4 at the small- x end (Coulomb singularity). This was to be expected since in both types of regions it is easily shown that $|\bar{v}_\theta| \ll |v_w|$ and $v_w/v \rightarrow 1$. For a box with an impenetrable wall the "tail" regions as we have just defined them consist merely of the $v = \infty$ regions outside the box; however, the lower left case in Fig. 3 has an approximate tail region near the center of the barrier, where the density is indeed quite low.

(iv) Overall, \bar{v} gives a much better approximation to the true v than does any combination of v_{TF} and v_w . However, \bar{v} still manifests some spurious oscillations,

and sometimes even has mild singularities, which we shall now discuss.

(v) All the \bar{v} plots of Fig. 3 are marred by cusplike singularities, which occur at the points x''_{\min} and x'_{\max} identified in Fig. 1; in Fig. 4, a singularity of this sort occurs at x''_{\min} , but not at x'_{\max} . As is shown in the Appendix, the occurrence of such singularities depends on the behavior of the function $\rho(x)$ at its left- or right-hand end: For the simple exponential decay characteristic of most physical problems (e.g., the large- x region of Fig. 4), no singularity occurs; for a quadratic decay to zero at a finite cutoff point (e.g., an impenetrable box wall or the $x=0$ Coulomb singularity), $d\bar{v}_\theta/dx$ becomes infinite as $(x - x''_{\min})^{-2/3}$ or $(x'_{\max} - x)^{-2/3}$; for harmonic oscillator problems, there is a weaker (logarithmic) divergence of $d\bar{v}_\theta/dx$.

(vi) The "box" examples in Fig. 3 show that \bar{v}_θ itself diverges near an impenetrable wall, the divergence being, as shown in the Appendix, inversely proportional to the distance from the wall, with a rather small coefficient. A similar negative divergence of v_θ occurs at $x \rightarrow 0$ in the Coulomb problem, but it is not very noticeable in Fig. 4 because the coefficient is much smaller than that occurring in the real potential v , as manifested in v_w (≈ 0.098 versus 1, for the case of Fig. 4).

B. Absolute level of \bar{v}_θ and its N dependence

Now let us focus attention on the absolute level of the potential curves in Figs. 3 and 4, i.e., their positions relative to the energy of the highest occupied state. We have already commented on the vanishing of v_{TF} in the tails where $\rho \rightarrow 0$ (the well-known zero ionization potential of simple Thomas-Fermi theory) and on the fact that in these tail regions adding to v_{TF} any fraction of v_w adds the same fraction of the difference between the true potential and the energy of the highest occupied state. We have also noted that our approximation \bar{v} to the potential eventually becomes correct in tails of exponential type, because $\bar{v}_\theta \rightarrow 0$ there. This is illustrated in the right-hand region of Fig. 4, which is the only exponential-tail region in our examples: As noted above, displacing the v curve upward by $\frac{1}{18}$ hartree (to shift its zero to the energy of the highest occupied state) would bring it very close to \bar{v} in this region. Indeed, the agreement is better than one would be justified in expecting on the basis of the reasoning of the Appendix. In the Gaussian tails of the harmonic-oscillator distributions of Fig. 3, \bar{v} runs parallel to v but does not coalesce with it, because, again as shown in the Appendix, \bar{v}_θ approaches a small constant value instead of zero. Percentage-wise, the error is small, however, as the total v is becoming quadratically infinite.

A spectacular consequence of our having defined the zero for v as the energy of the highest occupied state is that if one considers distributions $\rho(x)$ yielding nonintegral values of $N = \int \rho(x) dx$, the $v(x)$ curve must shift discontinuously when N increases through an integral value, since a new one-particle state begins to be occupied. Thus if we consider a sequence of ρ 's corresponding to closely spaced N values for distributions in a po-

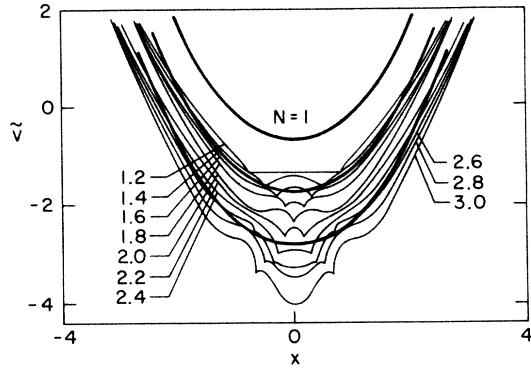


FIG. 5. Approximate potentials $\tilde{v}(x)$ calculated from (12) and (7) for densities corresponding to various nonintegral values of the number N of particles (of a single spin), for the harmonic-oscillator potential $v = \frac{1}{2}x^2 - \epsilon_{\max}$. Here ϵ_{\max} is the single-particle energy of the highest occupied state; the three heavy curves are the correct v 's for $\epsilon_{\max} = 0.5, 1.5,$ and 2.5 and hence should apply for $N \leq 1, 1 < N \leq 2,$ and $2 < N \leq 3,$ respectively. (Note that $\tilde{v} = v$ for $N \leq 1$.)

tential of given shape, the true v should remain fixed over the range $N + \epsilon$ to $N + 1$ (ϵ infinitesimal), and then shift uniformly downward at $N + 1 + \epsilon$. Figures 5 and 6 show to what extent our \tilde{v} follows this behavior, for harmonic-oscillator and Coulomb examples, respectively. We see that the \tilde{v} of the Coulomb problem does indeed show approximately the correct behavior in the tail region (large x); this is, of course, a consequence of the smallness of \tilde{v}_θ with respect to v_w here, and the fact that here ρ , and hence v_w , are dominated by the contribution from the highest occupied state. For the harmonic-oscillator problem \tilde{v} in the tails also seems to be approaching a discontinuous behavior, although its agreement with the exact v is marred by the small constant offset mentioned above. In the regions of large particle density, however, the variation of \tilde{v} as N goes from 2 to

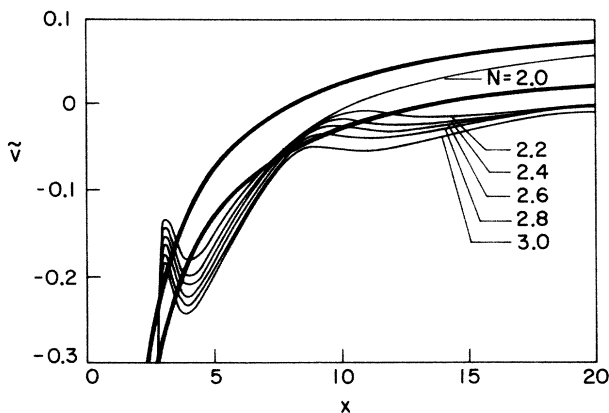


FIG. 6. Same as Fig. 5, for densities corresponding to various numbers N of particles in a Coulomb potential. Upper and lower dark curves refer to $N=2$ and 3 , respectively. (In comparing with Fig. 4, note that the convention of measuring v relative to ϵ_{\max} was not used there.)

3 become rather uniform for both systems with little sign of the proper discontinuous behavior. For the range $N=1$ to 2 , shown only in Fig. 5, the behavior is better, as \tilde{v} , which coincides exactly with v for $N \leq 1$, has already changed at $N=1.2$ to values that are closer to the curve for $N=2$, even in the central region.

Figures 5 and 6 provide a natural explanation for a pervasive defect in our approximate \tilde{v} curves, evident in Fig. 3 though less clear in Fig. 4. Namely, there is a tendency for \tilde{v} to lie, on the average, a little lower than the correct v . In sequences like those of Figs. 5 and 6 the true v remains constant as N increases toward an integer value N^* , and then shifts discontinuously downward to a new constant value as N passes through N^* . Any approximate \tilde{v} that varies continuously with N is therefore likely, if it gives approximately the right level for v on the average over a range of N , to be too low for $N < N^*$ and too high for $N > N^*$. Since our specification (24) of the reference level for v when $N = N^*$ is that obtaining at $N^* - 0$, \tilde{v} might be expected to lie usually too low.

C. Evaluation via v_θ alone

Thus far, in our comparisons of the potentials generated by our approximation (1) with the true ones or with those given by previous approximations, we have simply juxtaposed plots of v, \tilde{v} , etc., as functions of x . This is a natural thing to do, because the physical meaning of v needs no explanation and because any approximate kinetic-energy functional whatever can be made to yield a corresponding approximation to v by functional differentiation, as in (6) or (24). However, one of the facts pointed out in Ref. 1 was that the quantity T_θ defined by

$$T = T_w + T_\theta \quad (25)$$

is always greater than or equal to 0, as is T_w itself, so that it makes sense to focus on approximations that keep the term T_w and simply approximate T_θ . In such case the adequacy of this latter approximation is the only issue, and one should judge this comparing the \tilde{v}_θ derived from our approximate \tilde{T}_θ with the true v_θ , defined as $v - v_w$. Such a comparison can, however, be made for any approximation to T , regardless of whether it contains a full T_w term (e.g., the popular $T_{TF} + T_w/9$). As March⁸ has noted, the problem of finding an adequate approximation to the kinetic-energy functional T can be viewed as that of finding an adequate approximation to v_θ (the negative of his aptly named "Pauli potential").

Since comparisons of correct and approximate v_θ 's really give the same information as those of correct and approximate v 's, we shall present the former here for only three of the densities used in Fig. 3 and shall compare our approximation to v_θ only with the simple Thomas-Fermi form. These comparisons, given in Fig. 7, will suffice to illustrate one or two points more clearly than the presentation of Fig. 3. As in Fig. 3, all energies in Fig. 7 [except part (d)] are measured relative to the chemical potential, ϵ_F , i.e., the energy of the highest occupied one-particle state; thus the "correct v_θ " is

$$v_\theta(x) = v(x) - v_w(x) - \epsilon_F \quad (26)$$

and the Thomas-Fermi approximation is (23).

All parts of Fig. 7 show again the great superiority of our \bar{v}_θ over v_{TF} as an approximation to the true v_θ . What is particularly clear in panels (b)–(d) is that the oscillations in v_{TF} are almost exactly opposite in phase to those of the true v_θ , whereas those of \bar{v}_θ are in the correct phase, though not quite large enough. Of particular interest is the comparison of v_θ and \bar{v}_θ for four particles in a box, as this case begins to approximate that of an infinite gas of free fermions with a sinusoidal density modulation. Approximate correctness for the latter case in the linear-response limit was one of the criteria that guided the choice of the \bar{T} functional (1) in Ref. 1. As can be seen from Fig. 3 of that paper, no short-ranged functional is capable of fitting the correct linear-response behavior for wave numbers close to twice the Fermi wave number k_F where the correct linear-response function has a cusplike singularity. Indeed, the largest error in the \bar{T} function of (1) comes just at $2k_F$, and is sizable. For boxlike systems of finite size, hence a finite number of density oscillations, one might expect that what would be important would be an average over a range of wave vectors near $2k_F$, and for such an average the error should be less than that at exactly $2k_F$. In Fig. 7(d), where the systematic lowness of the \bar{v}_θ curve has been approximately eliminated by giving it an arbitrary upward shift, it can be seen that for four particles in a box the errors in the oscillatory part of \bar{v}_θ are modest, though appreciable.

IV. DENSITIES FOR SOME GIVEN POTENTIALS

A. Densities minimizing $\bar{T} + \langle v \rangle$

The effective potential \bar{v} , which we have plotted for various densities in Figs. 3 and 4, was defined in (6) as the negative variational derivative of our approximate

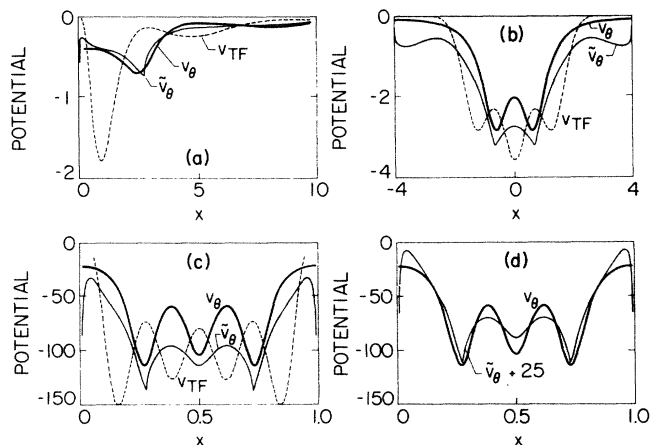


FIG. 7. Comparison of the correct v_θ function with the approximation \bar{v}_θ given by (12) and with the Thomas-Fermi approximation (23), for three sample densities: (a) three s electrons in a Coulomb field; (b) three particles in a harmonic-oscillator potential; (c) four particles in a box; (d) comparison of the v_θ curve of (c) with the \bar{v}_θ curve arbitrarily shifted upward by 25 units.

kinetic energy \bar{T} with respect to density. So if an infinitesimal number δN of particles are transferred from a region at x_1 to a region at x_2 , the change in $\bar{E} = \bar{T} + \langle v \rangle$, our approximation to the total energy, will be

$$\delta \bar{E} = \delta N [v(x_2) - \bar{v}(x_2) - v(x_1) + \bar{v}(x_1)] . \quad (27)$$

Thus if we start with a given $v(x)$ and a given trial density $\rho_0(x)$, a convenient way to construct a new density $\rho_1(x)$ that will give a lower \bar{E} will be to shift the $v(x)$ curve rigidly up or down until it has about the same average height as $\bar{v}(x)$, and then to increase ρ_0 slightly in regions where $(v - \bar{v})$ is negative and decrease it slightly where $(v - \bar{v})$ is positive; the integral $\int \rho dx$ must, of course, stay constant at the number N of particles we wish to study. The transfer δN must be kept small so that nonlinear effects will not upset the prediction that \bar{E} will be lowered; however, we can always calculate the new \bar{v} after the transfer, and repeat the whole process as often as necessary to achieve a convergence of \bar{v} to a form essentially equal to v , i.e., to minimize \bar{E} . We shall now describe our implementation of this procedure for three of the situations presented in Figs. 3 and 4; some intermediate stages will be illustrated for one of these problems in Fig. 8.

The first case undertaken was that of two particles (of a single spin) in a parabolic potential, for which the exact quantum-mechanical density was used to generate the curves of Fig. 3(c). A number of simple analytic forms for the density were tried, optimized with respect to parameters, and modified using the above comparison of \bar{v} with v . The density after several iterations was fairly close to the correct two-peaked $\rho(x)$ given by wave mechanics, but the dip at the center, relative to the two peaks on either side, was only about two thirds as deep as for the correct ρ .

A more careful test was undertaken for the case of three particles in a parabolic potential, that of Fig. 3(d). A simple algorithm was set up to convert any given trial density $\rho_1(x)$, normalized to three particles, into a slightly improved density $\rho_2(x)$, and this algorithm was iterated repeatedly by computer. We used a rather crude algorithm, consisting of the following steps: (i) calculate $\bar{v}(x)$ for the given $\rho_1(x)$, from (7) and (12); (ii) form the difference $\Delta v = v - \bar{v} - \Delta$, where v is the true potential and Δ is the mean of $v - \bar{v}$ weighted by ρ_1 ; (iii) form the new density

$$\rho_2(x) = \rho_1(x) [1 - \alpha \Delta v(x) / |\Delta v|_m] , \quad (28)$$

where α is a constant much less than 1 and $|\Delta v|_m$ is the maximum value of $|\Delta v|$ (note that ρ_2 will be normalized); and (iv) define $\rho_2(x)$ as a smoothed version of $\rho_2'(x)$. Only rather small values of α could be tolerated, so that many iterations were needed. (This appeared to be necessary to avoid instabilities due to repeated numerical differentiation and to the singularities in \bar{v}_θ noted in item (v) of Sec. III A.) The procedure proved rather inefficient. Nevertheless, an approximate convergence was achieved, with the results shown in Figs. 8 and 9. These suggest several conclusions. The idea of using

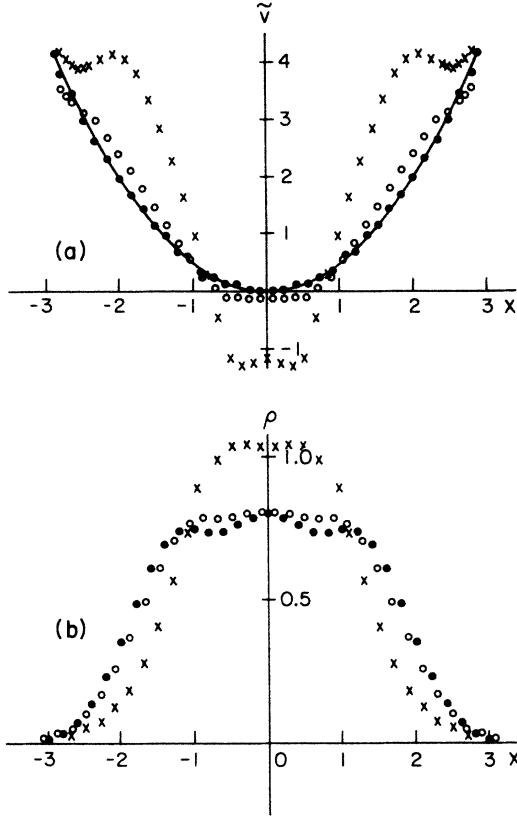


FIG. 8. Successive approximations to the density $\rho(x)$ minimizing $\tilde{T} + \langle V \rangle$ for the case of three parallel-spin particles in a harmonic potential $v = \frac{1}{2}x^2$. (a) The \bar{v} calculated from the initial approximation to $\rho(x)$ (crosses), that from a typical intermediate approximation (open circles), and that from the final approximation (filled circles), compared with the true v (solid curve); each approximation has been vertically shifted to make $\langle v - \bar{v} \rangle = 0$. (b) The corresponding three approximations to $\rho(x)$.

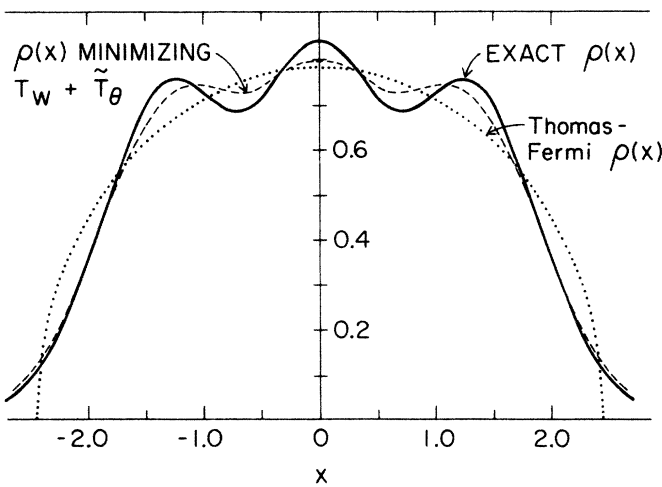


FIG. 9. Comparison of the "final" $\rho(x)$ of Fig. 8 (dashed curve—same as the black circles of Fig. 8) with the quantum-mechanical density for three parallel-spin particles in the parabolic potential (solid curve), and with the Thomas-Fermi density given by equating the right of (23) to $\frac{1}{2}x^2 - \epsilon_F$, with ϵ_F chosen to make $\int \rho dx = 3$ (dotted curve).

(28), or something like it, to iterate to self-consistency is supported by the fact that for densities departing sizably from the optimum, the calculated \bar{v} 's in the upper part of Fig. 8 cross the desired parabola at about the same x values as where the corresponding densities in the lower part of the figure cross the self-consistent one; similarly, large deviations of \bar{v} correspond roughly with large deviations of ρ . The final density—the one minimizing \tilde{E} —is, as Fig. 9 shows, very much closer to the true quantum-mechanical one than is the Thomas-Fermi density, which lacks both the central oscillations and the Gaussian tails. While inclusion of part or all of the Weizsäcker energy in the Thomas-Fermi model would improve the behavior in the tails, it would never—as we shall prove in Sec. IV B below—yield multiple local maxima in the density. Our solution tracks the true solution closely in the tail regions, but the central oscillations are, as for the two-particle case, not sufficiently pronounced. This defect is doubtless related to the fact that the expression (1) we have adopted for \tilde{T} yields a much less pronounced minimum at wave vector $2k_F$ in the linear-response function for small departures from a nearly uniform ρ than does wave mechanics (see Figs. 3 of Ref. 1).

A final comparison of a density minimizing \tilde{E} with the corresponding quantum-mechanical density was made for the case of three particles (of a single spin) in the s states of a Coulomb potential, i.e., the case used for Figs. 4, 6, and 7(a). For this case we were not successful in designing an adequate algorithm for a fully automated iteration to self-consistency, probably mainly because the singularity in \bar{v}_θ noted in Sec. III A is, as detailed in the Appendix, more pronounced than that for the harmonic oscillator. Having found that simple iterations based on (28) failed to converge adequately, we tried the alternative iteration scheme of determining a new trial density ρ'_2 from an initial density ρ_1 via

$$v_w\{\rho'_2; x\} = v(x) - \bar{v}_\theta(\rho_1; x), \quad (29)$$

an equation which by (7) amounts to a Schrödinger-type equation for the "wave function" $(\rho'_2)^{1/2}$. (This has also been suggested by Levy *et al.*² as a broadly applicable procedure.) However, we found that to avoid divergences the new approximation ρ_2 had to be taken much closer to ρ_1 than to the ρ'_2 determined from (29), and in spite of further experimentation along these lines we were unable to get a satisfactory convergence. Since our goal was merely to get a self-consistent density for this one problem, and not to develop a general algorithm for use with the present arbitrarily chosen \tilde{T} functional for the practically unimportant case of one-dimensional problems, we decided to seek self-consistency by a succession of hand-picked modifications to the density.

Figure 10 shows the results. There is, of course, no sign of shell structure in the Thomas-Fermi density, and we may note that, according to the theorem to be proved in Sec. IV B, no kinetic-energy functional made up by adding various (positive) amounts of Thomas-Fermi and Weizsäcker energies could yield a nonmonotonic density for the present problem. Use of the \tilde{T} of (1), on the other hand, yields a weak but real peak in

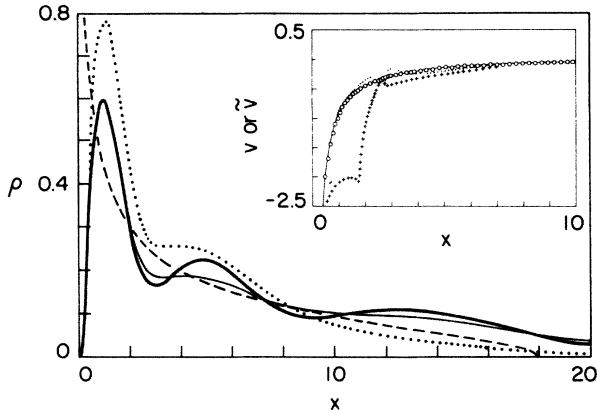


FIG. 10. Various approximations to the radial density $\rho(x)$ for the problem of three parallel-spin particles ($\int \rho dx = 3$) in the lowest s states of a Coulomb potential. Dark curve, quantum solution. Light solid curve, density approximately minimizing $\tilde{T} + \langle V \rangle$. Dashed curve, Thomas-Fermi density. Dotted curve, a sample trial function used in an unsuccessful iteration scheme, obtained as the eigenfunction of a Schrödinger-type equation of the form (29). Inset, comparison of the potentials $\bar{v}_\theta + v_w$ calculated for three of the densities with the true potential $v = -(1/x) + \frac{1}{18}$ (dark curve). Open circles, dots, and crosses refer, respectively, to the density approximately minimizing $\tilde{T} + \langle v \rangle$, the correct quantum-mechanical density, and the non-optimal sample density, respectively. (Note that the latter shows singularities in its \bar{v} both where $\int_0^x \rho_1 dx = 1$ and where $\int_0^x \rho_2 dx = 1$.)

$\rho(x)$ near the proper position for the $2s$ shell and although it does not quite produce a peak in the $3s$ region, it does produce a quite noticeable shoulder there. Thus the conclusion from Fig. 10 is similar to that from Fig. 9: Our approach yields density oscillations of the right sort, but these are insufficiently pronounced, doubtless because in the linear-response limit our \tilde{T}_θ does not adequately reproduce the depth and sharpness of the minimum at $2k_F$ in the correct linear-response function. Again, the upper right of Fig. 10 shows that the comparison of the \bar{v} derived from a trial density ρ_T will typically differ considerably from the true v whenever ρ_T differs sizably from the correct ρ , i.e., that our self-consistency criterion is a reasonably sensitive measure of the correctness of ρ_T .

Note that in the language of the Schrödinger-type equation (26) or (29), local maxima and minima in $\rho(x)$ must be associated with sufficiently strong minima and maxima, respectively, in the effective potential $v - v_\theta$, and hence will often correlate with maxima and minima, respectively, of v_θ . As Fig. 7 shows, our \bar{v}_θ often has roughly the right pattern of such extrema.

B. Theorem on densities derived from Thomas-Fermi-Weizsäcker functionals

We shall now show that if the relation between density and potential is assumed to have any form made up from the Thomas-Fermi and Weizsäcker expressions, it

is impossible for a potential well with only a single minimum to give rise to a density with multiple maxima. More precisely, we postulate that the kinetic energy is given by a functional

$$T_{TFW} = w_{TF} T_{TF} + w_w T_w, \quad (30)$$

where w_{TF} and w_w are each greater than or equal to 0, T_{TF} is the Thomas-Fermi energy,

$$T_{TF}\{\rho\} = \frac{\pi^2}{6} \int \rho^3 dx, \quad (31)$$

and T_w is the Weizsäcker energy given by (2); we assume all particles to have the same spin. The density ρ minimizing the sum of the kinetic energy (30) and the potential energy $\langle V \rangle = \int \rho v dx$ in a given external potential $v(x)$ will then obey

$$v(x) = w_{TF} v_{TF}(x) + w_w v_w(x), \quad (32)$$

where v_{TF} is given by (23) and v_w by (7).

Now suppose that ρ has a local maximum at some point x_{\max} and a local minimum at some other point x_{\min} . Then with only the first term of (7) contributing,

$$v_w(x_{\max}) < 0 < v_w(x_{\min}), \quad (33)$$

while

$$v_{TF}(x_{\max}) < v_{TF}(x_{\min}), \quad (34)$$

so (32), (33), and (34) require that

$$v(x_{\max}) < v(x_{\min}). \quad (35)$$

If ρ has more than one local maximum, there must be a sequence of points $x_{\max}^{(1)} < x_{\min} < x_{\max}^{(2)}$ between which v first increases, then decreases. This is impossible if v has just a single minimum on either side of which it rises monotonically. For such a potential, therefore, ρ can have only one local maximum.

Minor generalizations of this theorem can easily be made. For the attractive Coulomb potential, for example, $v \rightarrow -\infty$ at one end of the allowed range of x ; its monotonic increase with x is inconsistent with the existence of a maximum in ρ away from $x=0$, if (30) is assumed. In three dimensions, too, where $T_{TF} \propto \int \rho^{5/3} dx$ and T_w involves $\nabla^2 \rho$ and $|\nabla \rho|^2$, the kinetic energy again requires that v at a local maximum in ρ be less than v at a contiguous local minimum.

V. CONCLUSIONS

The most important message of the present paper is its strengthening of the general conclusion of Ref. 1, that it is possible to obtain usefully accurate approximations to the true kinetic-energy functional of noninteracting fermions by interpolations that possess, or nearly possess, the correct behavior both in the limit of nearly uniform density and in the limit where certain regions containing not more than one particle of a given spin become isolated from the rest of the distribution. We have illustrated this possibility by calculations using a specific interpolation functional, namely, that given by Eq. (1),

for one-dimensional problems. These calculations have revealed some virtues of the expression (1), some defects of it, and some serious shortcomings of some alternative approximations to the kinetic energy that fail to fit the two limiting-case criteria just mentioned.

In terms of the nonlocal relation between particle density ρ and external potential v , i.e., the functional $v\{\rho\}$ or $\rho\{v\}$, we may describe virtues or defects of any approximation such as (1) in terms of comparisons of the functionals $\bar{v}\{\rho\}$ or $\bar{\rho}\{v\}$ to which it leads with the correct quantum-mechanical functionals. Virtues of (1), which could presumably be duplicated or improved by other approximate functionals constructed according to the same philosophy, include asymptotically correct representation of $v\{\rho\}$, and near correctness of $\bar{\rho}\{v\}$, in the decaying tails of a distribution; nearly correct $\bar{v}\{\rho\}$ or $\bar{\rho}\{v\}$ near a Coulomb singularity of the potential; fairly reasonable $\bar{v}\{\rho\}$ over the whole range for a wide variety of problems; and a $\bar{\rho}\{v\}$ that shows Friedel oscillations (or shell structure) roughly though not accurately in accordance with the correct quantum-mechanical ones.

Defects of the functional (1) include the fact that the just-mentioned oscillations in $\bar{\rho}\{v\}$ come out somewhat too weak for typical few-particle problems with rapid variation of v near the "walls" of the potential well; its failure to approximate the discontinuous jump of $\bar{v}\{\rho\}$, measured relative to the highest occupied level, when the particle number N_s for spin s changes through an integer value, except for N_s near 1 or in the tails of the distribution; and the fact that for some problems in which v becomes infinite $\bar{v}\{\rho\}$ can have spurious weak singularities (usually just in its derivative, but for rigid-wall potentials also in its magnitude). All of these defects could doubtless be ameliorated by making reasonably tractable modifications in the \bar{T} of (1). For example, the first two defects (re oscillations and discontinuities, respectively) would probably be helped by allowing the \bar{T} functional to depend not only on a remoteness variable like the ξ of (5), but also on similar variables defined for two-particle, three-particle, etc., intervals. Similarly, modification of the definition of ξ might eliminate the occasional singular behavior of $\bar{v}\{\rho\}$. However, as was pointed out in Ref. 1, pursuit of such improvements for one-dimensional problems is probably of less interest at this time than the search for tractable kinetic-energy functionals in three dimensions.

In the present paper the performance of the approximation (1) to the kinetic-energy functional has been compared with that of only one category of alternative approximations, namely, those that represent the kinetic energy as a linear combination, with positive coefficients, of a Thomas-Fermi term T_{TF} and a Weizsäcker term T_w , i.e., for one-dimensional cases, of the expressions (31) and (2). Such combinations, particularly ones using a coefficient unity for the Thomas-Fermi term, have been very popular in the previous literature.⁹ However, our examples show that all such choices for the approximate functional \bar{T} in one dimension yield far worse results than our expression (1), in that, in cases where ρ has Friedel-type oscillations, they yield $\bar{v}_\theta\{\rho\}$, whose oscillations tend to be opposite in phase to those of the correct

$\bar{v}_\theta\{\rho\}$, so that $\bar{v}\{\rho\}$ acquires large spurious oscillations, which become worse the larger the coefficient of T_w ; they never yield Friedel or shell-structure oscillations in $\bar{\rho}\{v\}$ if v has a simple single minimum; they yield $\bar{v}\{\rho\}$ and $\bar{\rho}\{v\}$ with wrong behavior in the tails of the distribution if the coefficient of T_w is other than unity; and they always yield a $\bar{v}\{\rho\}$ that varies smoothly with N , even near $N=1$, though correct behavior can be achieved in the tails if the coefficient of T_w is unity.

Other approximate kinetic-energy functionals have been proposed, which we shall not attempt to discuss in detail. However, a few general comments are in order. Local functionals,¹⁰ which approximate the kinetic energy as an integral of some function of ρ and its derivatives at each point, can never yield a $\bar{v}\{\rho\}$ that behaves reasonably for all densities ρ . For such $\bar{v}\{\rho\}$ must also be local functionals and hence must, over any range of coordinate space containing less than one particle of a single spin, coincide with the $\bar{v}\{\rho_1\}$ for the ρ_1 of a one-particle problem so defined that $\rho_1=\rho$ over this region. If the assumed functional and its \bar{v} are to be good approximations when the density is ρ_1 , then $\bar{v}\{\rho_1\}$ must be close to $v_w\{\rho_1\}$, where v_w , given in one dimension by (7), is the functional derivable from the approximation $\bar{T}=T_w$. As our many examples have shown,¹¹ such an approximation would be very bad for most many-particle distributions.

In parallel with the recent spurt of interest in nonlocal exchange-correlation functionals, some explicit nonlocal kinetic-energy functionals have been studied by Alonso and Girifalco¹² and by Plumer and Geldart.¹³ The latter authors recognized the need for nonlocality and the utility of the linear-response function of the uniform Fermi gas as a guide to setting up an appropriate nonlocal theory. However, the kinetic-energy functionals they chose for study have the form of T_w+T_{TF} plus a generally negative nonlocal correction $G_\gamma\{\rho\}$ expressible as an energy associated with each pair of points r, r' . Qualitative considerations based on our criteria support the conclusion they reached from numerical studies of atomic examples, that such functionals are rather inadequate. It would be hard to make a G_γ of this form behave properly, e.g., to reduce to $-T_{TF}$ for one-particle problems, or to undo the huge spurious oscillations in $\bar{v}\{\rho\}$ which T_w+T_{TF} would give for typical several-particle problems. Note too that their procedure would give rather poor results for $\bar{v}\{\rho\}$ for cases like Fig. 3(e) where adjacent high-density regions are separated by a weakly penetrable barrier. What one must do is rather to *replace T_{TF} in its entirety by a nonlocal expression*, as our form (1) does.

ACKNOWLEDGMENT

This work was supported by the National Science Foundation Materials Research Laboratory (NSF-MRL) Program through the Center for Materials Research at Stanford University.

**APPENDIX: SINGULARITIES
AND ASYMPTOTIC BEHAVIOR OF $\bar{v}_\theta(x)$
FOR CERTAIN TYPES OF DENSITIES**

We wish to examine possibilities for the expression (12) for $\bar{v}_\theta(x)$ to become infinite, or to have an infinite derivative. For the former possibility to occur, a ρ in one of the denominators would have to go to zero. However, this produces no divergence in the second of the terms arising from the first square bracket, if ρ is approaching zero as $|x - x_0|^\alpha$ with $\alpha \geq 2$, or as $e^{-\lambda|x|}$ or $e^{-\lambda x^2}$, since in all such cases the factor $[\xi_1(\bar{x})]^4$ in the denominator compensates the behavior of $\rho(x')$ or $\rho(x'')$. These cases cover behavior near an impenetrable wall or a Coulomb singularity, and the behavior at infinity in a finite or parabolic potential. The contribution from the first term in the first square bracket is likewise innocuous.

Thus for the sorts of problems we have been considering, an infinite $\bar{v}_\theta(x)$ can arise only from $\rho(x)$ approaching zero in the last term of (12). Consider first the case $\rho \sim a(x - x_0)^\alpha$, $x > x_0$. For this case the height of the hatched region of Fig. 1(b) becomes zero at the left end, where $x = x_0$ and $\bar{x} = (x_0 + x''_{\min})/2$. If x varies over some small range near x_0 , (4) implies that x'' varies very little in comparison with the variation of x' , so long as $\rho(x'')$ is not especially small. Thus

$$\bar{x} \sim (x' + x''_{\min})/2, \quad d\bar{x} \sim dx'/2, \quad (\text{A1})$$

$$\Delta x \sim (x''_{\min} - x_0), \quad (\text{A2})$$

$$x_a(x) \sim (x_0 + x''_{\min})/2, \quad x_b(x) \sim (x + x''_{\min})/2 \quad (\text{A3})$$

and by (5)

$$\xi_1^2 \sim (x' - x_0)^{1-\alpha}/a(1-\alpha) + O(1). \quad (\text{A4})$$

With $y = x' - x_0$, we can now write, for x near x_0 ,

$$\begin{aligned} \text{Last integral in (12)} &\sim \frac{a^2(1-\alpha)^2}{2(x''_{\min} - x_0)} \int_0^{x-x_0} \frac{dy}{y^{2-2\alpha}} \\ &= \frac{a^2(1-\alpha)^2(x-x_0)^{2\alpha-1}}{2(2\alpha-1)(x''_{\min} - x_0)}. \end{aligned} \quad (\text{A5})$$

Because of the $[\rho(x)]^{-2}$ multiplying this in (12), (12) will be dominated by its last term, so that as $x \rightarrow x_0$,

$$\bar{v}_\theta(x) \sim - \frac{\pi^2(1-\alpha)^2}{12(2\alpha-1)(x''_{\min} - x_0)(x - x_0)}. \quad (\text{A6})$$

An analogous expression, of course, results for the symmetrical case $\rho \sim a(x_0 - x)$, $x < x_0$. In the Coulomb problem and at an impenetrable wall we have $\alpha = 2$, so (A6) reduces to $-\pi^2/36(x''_{\min} - x_0)(x - x_0)$. Since the correct $v_\theta(x)$ for such problems is easily shown to be finite as $x \rightarrow x_0$, this divergence, though weak, is a defect of the approximation used in the present paper.

For the more realistic class of problems where $\rho \sim be^{\lambda x}$ as $x \rightarrow -\infty$, or $\rho \sim be^{-\lambda x}$ as $x \rightarrow \infty$, \bar{v}_θ remains finite. For the former case, for example, (A1) still applies, and we have

$$\Delta x \sim (x''_{\min} - x'), \quad (\text{A7})$$

$$\xi_1^2 \sim e^{-\lambda x'}/b\lambda, \quad (\text{A8})$$

$$\text{last integral in (12)} \sim b^2\lambda e^{2\lambda x}/4(x''_{\min} - x). \quad (\text{A9})$$

Since the terms arising from the first square bracket in (12) are exponentially small as $x \rightarrow -\infty$, we have in this limit

$$\bar{v}_\theta(x) \sim -\pi^2\lambda/24(x''_{\min} - x), \quad (\text{A10})$$

so that \bar{v}_θ behaves qualitatively like the correct v_θ which must go to zero in the exponential tails of the distribution,⁷ though the algebraic decay of (A10) is not as fast as the true decay should be.

Similar reasoning can be carried through for cases, like the harmonic oscillator problem, where $\rho \sim be^{-\lambda x^2}$. The result for this case is that \bar{v}_θ approaches a finite limit as $|x| \rightarrow \infty$. Since $v_w \rightarrow \infty$ as x^2 , \bar{v}_θ becomes much less than v_w , but it does not approach zero as the correct v_θ should.

Singularities in the derivative of \bar{v}_θ may occur when $x = x''_{\min}$ or x''_{\max} (see Fig. 1), since at these points the derivative of (12) involves dx_a/dx or dx_b/dx , which becomes infinite. For most physically realizable situations, where ρ decays at infinity as $be^{\pm\lambda x}$, no infinity in $d\bar{v}_\theta/dx$ actually occurs, because the integrands go to zero at the limit of integration, and do so sufficiently rapidly to more than compensate the divergence of dx_a/dx or dx_b/dx . But for impenetrable-wall cases the balance is less favorable. Consider the case where x is just to the right of x''_{\min} in Fig. 1(b), so that when \bar{x} is near x_a , x' is near x_{\min} ; here let

$$\rho(x') \sim a(x' - x_{\min})^2, \quad (\text{A11})$$

a behavior applicable both to impenetrable-wall problems and to the Coulomb problem. From the definition of x_a in Fig. 1 we have

$$\frac{dx_a}{dx} = \frac{d\bar{x}}{dx''} \sim \frac{1}{2} \frac{dx'}{dx''} \sim \frac{\rho(x'')}{2\rho(x')} \sim \frac{\rho(x''_{\min})}{8a(\bar{x} - \bar{x}_{\min})^2}. \quad (\text{A12})$$

In the integrands of (12) we have

$$\Delta x \sim (x''_{\min} - x_{\min}), \quad (\text{A13})$$

$$\xi_1^2 \sim 1/a(x' - x_{\min}) \sim 1/2a(\bar{x} - \bar{x}_{\min}), \quad (\text{A14})$$

$$\text{Integrand} \sim \frac{a}{(x''_{\min} - x_{\min})\rho(x''_{\min})}. \quad (\text{A15})$$

Multiplying (A12) and (A15) and including the factor $-\pi^2/6$, we have for the asymptotic behavior of (12)

$$\frac{d\bar{v}_\theta}{dx} \sim \frac{\pi^2}{48(x_a - \bar{x}_{\min})^2}. \quad (\text{A16})$$

Here x_a is determined by

$$\begin{aligned} \rho(x''_{\min})(x - x''_{\min}) &\sim \int_{x_{\min}}^{x'(\bar{x}=x_a)} a(x_1 - x_{\min})^2 dx_1, \\ &= \frac{a}{3}(x' - x_{\min})^3 \sim \frac{8a}{3}(x_a - \bar{x}_{in})^3. \end{aligned} \quad (\text{A17})$$

Thus finally

$$\frac{d\bar{v}_\theta}{dx} \sim \frac{\pi^2}{12 \times 3^{2/3}} \left[\frac{a}{\rho(x''_{\min})(x - x''_{\min})} \right]^{2/3}. \quad (\text{A18})$$

This describes the singularities in Figs. 3 and 4, except

for the harmonic-oscillator cases. For the latter, the asymptotic behavior of $\rho(x)$ as $x \rightarrow -\infty$ is proportional to $x^{2n} e^{-\lambda x^2}$, where $(n+1)$ is the quantum number of the highest occupied state. Repetition of steps analogous to (A12)–(A18) gives

$$\frac{dx_a}{dx} \sim \text{const} \times e^{\lambda(x')^2} / (x')^{2n}, \quad (\text{A19})$$

$$\text{First integrand in (12)} \sim \text{const} (x')^{2n+1} e^{-\lambda(x')^2}, \quad (\text{A20})$$

$$\frac{d\bar{v}_\theta}{dx} \sim \text{const} |x'(\bar{x}=x_a)| \sim \text{const} \cdot \ln(x - x''_{\min}). \quad (\text{A21})$$

The singularity is thus weaker than that of (A18).

¹C. Herring, Phys. Rev. A **34**, 2614 (1986).

²M. Levy, J. P. Perdew, and V. Sahni, Phys. Rev. A **30**, 2745 (1984).

³Ref. 1, Sec. IV and Appendix B.

⁴Ref. 1, Sec. III B.

⁵N. H. March, Phys. Rev. A **33**, 88 (1986).

⁶J. P. Perdew, R. G. Parr, M. Levy, and J. L. Balduz, Phys. Rev. Lett. **49**, 1691 (1982); see also Ref. 1, Sec. II A.

⁷Ref. 1, Sec. II C.

⁸N. H. March, Phys. Lett. **113A**, 66 (1986); **113A**, 476 (1986).

⁹For a representative evaluation and further references, see C.

Q. Ma and V. Sahni, Phys. Rev. B **16**, 4249 (1977).

¹⁰See, for example, H. B. Huntington, Phys. Rev. B **20**, 3165 (1979); R. Baltin, J. Phys. A **20**, 111 (1987).

¹¹See also Table I of Ref. 1 for typical comparisons of T_w with $\langle T \rangle$.

¹²J. A. Alonso and L. A. Girifalco, Phys. Rev. B **17**, 3735 (1978).

¹³M. L. Plumer and D. J. W. Geldart, J. Phys. C **16**, 677 (1983). We are indebted to Dr. Plumer for calling this work to our attention.